Rev.Adv.Mater.Sci. 4 (2003) 1-9

POLYMER SURFACTANT INCORPORATED CERAMIC OXIDE NANOPARTICLES

S. Shukla[1] , S. Seal[1], R. Vij[2] and S. Bandyopadhyay[2]

[1] Advanced Materials Processing and Analysis Center (AMPAC) and Mechanical Materials Aerospace Engineering Department (MMAE), 4000 Central Florida Blvd., University of Central Florida, Orlando, Florida 32826, U.S.A.

[2] School of Materials Science and Engineering, University of New South Wales, NSW 2052, Australia

Received: November 04, 2002

Abstract. Sol-gel technique utilizing hydroxypropyl cellulose (HPC) polymer as a steric stabilizer, has been used to synthesize nanocrystalline zirconia (ZrO_2) powder. Various analytical techniques such as transmission electron microscopy (TEM), high-resolution TEM (HRTEM), scanning electron microscopy (SEM), x-ray photoelectron microscopy (XPS) and x-ray diffraction (XRD) are used to characterize the as-synthesized and calcined nanocrystalline ZrO_2 powder. The high temperature metastable tetragonal phase stabilization in undoped nanocrystalline ZrO_2 particles is studied in view of three different phase stabilization mechanisms. It is revealed that these phase stabilization mechanisms operate depending on the average ZrO_2 nanoparticle size within the as-synthesized nano-sized ZrO_2 powder, which in turn can be effectively controlled by adjusting the sol-gel processing parameters involving the ratio of molar concentrations of water and zirconium (IV) n-propoxide (R), the concentration [HPC] and the molecular weight (MW_{HPC}) of the HPC polymer. The variation in the relative volume fraction of tetragonal phase (V_T) as a function of R and [HPC] is explained on the basis of variation in the average ZrO_2 nanoparticle size and the operation of dominant metastable tetragonal phase stabilization mechanism as a function of R and [HPC].

1. INTRODUCTION

Zirconia (ZrO_2) is a well-known ceramic oxide material used for variety of applications such as a dispersed phase [1], catalyst/catalyst support [2], membrane [3], and sensor [4]. It is now well recognized that the mechanical, electrical, chemical as well as catalytic properties of ZrO_2 can be improved using nanocrystalline instead of conventional micron-sized zirconia. Synthesizing nanocrystalline ZrO_2 with metastable tetragonal (and cubic) phase(s) at room temperature thus plays an important role. In this report, we review our own new results [5-9] related to nanocrystalline tetragonal-ZrO_2 powder synthesis using sol-gel technique, which utilizes hydroxypropyl cellulose (HPC) polymer as a steric stabilizer.

2. EXPERIMENTAL

Pure zirconium (IV) n-propoxide, anhydrous ethanol (200 proof), and the HPC polymer (molecular weight: 80000, 100000, 370000 and 1000000 g/mol) were obtained from Aldrich Co. U.S.A. and used as received. Nanocrystalline ZrO_2 powder was synthesized via hydrolysis of zirconium (IV) n-propoxide in an alcohol solution [5]. The beakers used in the experiments were cleaned, washed with de-ionized water, dried completely and rinsed with anhydrous 200 proof ethanol before use. During synthesis, two different but equal parts of alcohol solutions were prepared. In the first part, de-ionized water was dissolved into anhydrous 200 proof ethanol in a specific proportion. An appropriate amount of the HPC polymer was then added and dissolved completely by stirring the solution overnight using a magnetic stirrer. The second part of the alcohol solution was

Corresponding author: S. Seal, e-mail: sseal@pegasus.cc.ucf.edu

then prepared by completely dissolving a specific amount of zirconium (IV) n-propoxide (this amount was kept constant for all experiments involved in this investigation) in an anhydrous 200 proof ethanol under atmospheric conditions. The solution was homogenized using magnetic stirring for few minutes only. After preparing each solution, both the beakers were sealed immediately with paraffin tape. Hydrolysis of zirconium (IV) n-propoxide was then carried out under atmospheric condition by rapidly mixing the two sealed solutions under vigorous stirring. The formation of ZrO_2 particles, due to immediate precipitation, was evident from the white color of the resulting sol. The sol was stirred very slowly for 4 h and then held under static condition for 24 h to ensure completion of the hydrolysis and the condensation reactions. The sol was subsequently dried at 80 °C using petri dishes in order to remove the solvent completely. The small gel pieces obtained were then crushed to obtain the nano-sized ZrO_2 powder.

The nano-sized ZrO_2 powder was synthesized using the above method under various processing conditions by varying the ratio of molar concentrations of water and zirconium (IV) n-propoxide (*R*), the concentration [HPC] and the molecular weight (MW_{HPC}) of the HPC polymer [5,6,7]. The concentration (0.1 M) of zirconium (IV) n-propoxide was kept constant for all experiments. The values of *R*, [HPC] and MW_{HPC} were respectively varied as: *R*=5, 15, 30, 60, [HPC]=0.0, 1.0, 2.0 g/l (Note: Unless otherwise stated, the MW_{HPC} of 80000 g/mol can be assumed for all results). The nano-sized ZrO_2 powder synthesized under different processing conditions was calcined at different temperatures ranging from 200-1200 °C in air for the phase evolution study. The samples were heated at a rate of 30 °C/min up to the calcination temperature, held at that temperature for 2 h, and then furnace cooled to room temperature.

3. CHARACTERIZATION

The as-synthesized nano-sized ZrO_2 powders were then examined using Phillips EM400 transmission electron microscope (TEM) at 120 kV to determine the nanoparticle size. High-resolution field TEM (HRTEM) (FEI-Philips Tecnai F30) was used to observe lattice images showing different orientations of nanocrystals within a sub-micron sized ZrO_2 particle, after calcination at 400 °C for 2 h. Bright field and dark field TEM images at 300 kV were taken to observe the lattice. Selected-area electron diffraction (SAED) patterns were taken to analyze the crystal structure. SAED patterns, collected near the edge and from the center of the particle, provided the presence of nanocrystals within a sub-micron sized particle. The surface chemistry of nano-sized ZrO_2 powder, in the as-synthesized and calcined conditions, was studied with the help of 5400 PHI ESCA (x-ray photoelectron spectroscopy (XPS)) spectrometer having a base pressure of $5 \cdot 10^{-9}$ Torr, using Mg K_α X-radiation (1253.6 eV), at a power of 350 watts. Both the survey and the high-resolution narrow spectra were recorded with electron pass energy of 44.75 eV and 35.75 eV respectively to achieve the maximum spectral resolution. The binding energy (B.E.) of the Au $4f_{7/2}$ at 84.0±0.1 eV was used to calibrate the B.E. scale of the spectrometer. Any charging shifts, produced by the nano-sized ZrO_2 powder synthesized in the presence of HPC polymer, were carefully corrected using the C (1s) B.E. of the C-H bond (285.0 eV) within the HPC polymer [10]. For the nano-sized ZrO_2 powder, synthesized in the absence of HPC polymer, charging shifts are corrected using the C (1s) B.E. (284.6 eV) of adventitious carbon [11]. Non-linear least square curve fitting was performed using a Gaussian/Lorentzian peak shape after background removal [12]. The crystalline phases present in the as-synthesized as well as calcined powders were determined using a standard Rigaku x-ray diffractometer (XRD). Line traces were obtained over 2-θ values ranging from 10°-80°. The volume fractions of tetragonal (V_T) and monoclinic (V_M=1-V_T) phases were calculated from the broad scan analysis considering the relative intensities of one tetragonal $(111)_T$ and two monoclinic peaks $(-111)_M$ and $(111)_M$ peaks and then using the relationship of the form [13]:

$$V_T = I(111)_T / [I(111)_T + I(-111)_M + I(111)_M]. \quad (1)$$

Narrow scan analysis was conducted in the 2-θ range of 27°-32° as it contained the strongest lines for monoclinic $(-111)_M$ as well as tetragonal $(111)_T$ phases. These intense peaks were then curve-fitted using the peak-fit software (peak-fit, version-4, SPSS Inc.). The average tetragonal (D_T) and monoclinic (D_M) crystallites size were calculated from the $(111)_T$ and $(-111)_M$ diffraction peaks using Scherrer's equation [14].

4. RESULTS

Typical TEM images of nano-sized ZrO_2 powder, synthesized via sol-gel method under the various processing conditions, are presented in Fig. 1. Submicron sized (~200 nm), near-spherical ZrO_2 particles are observed under the synthesis conditions

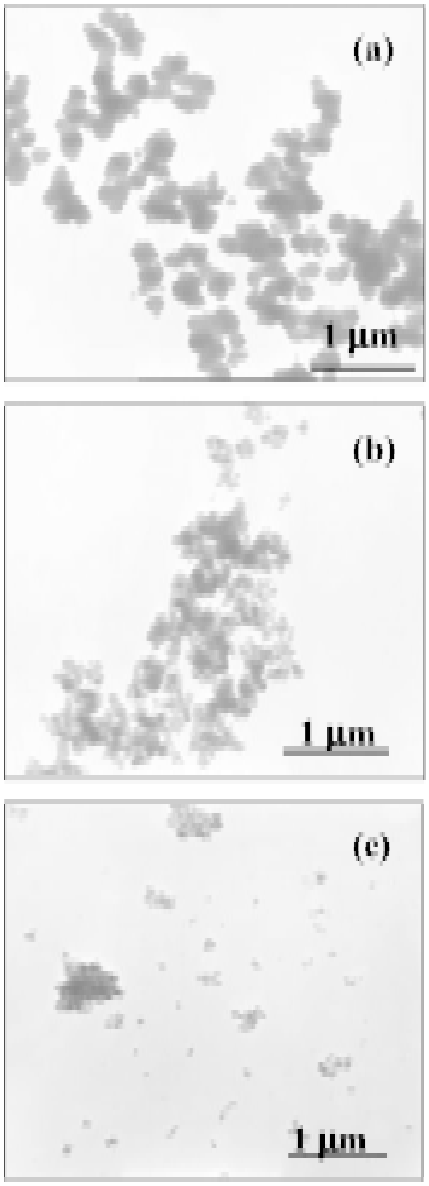

Fig. 1. Typical TEM images of sol-gel synthesized nano-sized ZrO_2 powders: (a) *R*=5, [HPC]=0.0 g/l, (b) *R*=30,[HPC]=0.0 g/l, and (c) *R*=30,[HPC]=2.0 g/l.

of *R*=5/[HPC]=0.0 g/l, Fig. 1(a). Agglomeration of these sub-micron sized ZrO_2 particles is noted under these processing conditions. In Fig. 1(b), ZrO_2 nanoparticles are synthesized under the processing conditions of *R*=30/[HPC]=0.0 g/l. Comparison of Figs. 1(a) and 1(b) shows that average ZrO_2 nanoparticle size is reduced due to increase in the *R*-value from 5 to 30. ZrO_2 nanoparticles in Fig. 1(b) are also observed to be agglomerated and form 'weak-agglomerates' under the processing conditions of *R*=30/[HPC]=0.0 g/l. In Fig. 1(c), ZrO_2 nanoparticles are synthesized under the processing conditions of *R*=30/[HPC]=2.0 g/l. Comparison of Figs. 1(b) and 1(c) shows that not only the average ZrO_2 nanoparticle size is decreased further but also the agglomeration tendency of ZrO_2 nanoparticles is reduced considerably due to the addition of HPC polymer ([HPC]=2.0 g/l) during processing.

The XPS broad scans obtained for the sol-gel derived (*R*=30,[HPC]=2.0 g/l) nano-sized ZrO_2 powder, in the as-synthesized and calcined (800° C for 2 h) conditions, are presented in Figs. 2(a) and 2(b) respectively. The corresponding narrow scan analysis of C (1s) spectrum, within the B.E. range of 270-300 eV, is shown in Figs. 3(a) and 3(b), respectively. In Fig. 2(a), the presence Zr, O, and C are detected on the ZrO_2 powder surface. Variation in the relative intensities of the respective peaks is also noted as a result of the calcination of the as-synthesized nano-sized ZrO_2 powder at 800 ° C for 2 h, Fig. 2(b). Comparison of Figs. 3(a) and 3(b) shows that the FWHM of C (1s) spectrum decreases as a result of calcination at higher temperature. Further, the deconvolution of the C (1s) spectra reveals that the C(1s) spectrum related to the as-synthesized powder, Fig. 3(a), is composed of three sub-peaks located at the B.E. positions of 285.0 eV, 286.4 eV, 289.7 eV and are identified as C-H, (C-O-H, C-O-C), and C=O bonds respectively, which are the finger prints of the HPC polymer [15]. On the other hand, only one sub-peak, located at the B.E. position of 284.6 eV, is identified in the calcined powder, Fig. 3(b).

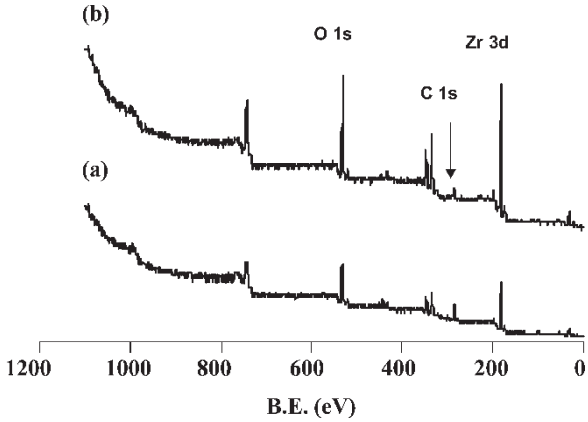

Fig. 2. XPS broad scan analysis of sol-gel derived ZrO_2 nanoparticles (*R*=30,[HPC]=2.0 g/l): (a) as-synthesized and (b) calcined at 800 °C for 2 h.

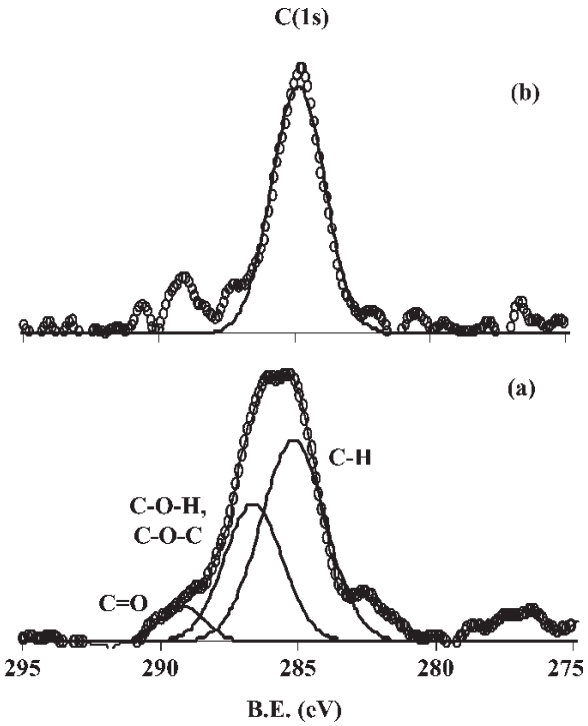

Fig. 3. XPS narrow scan C (1s) analysis of sol-gel derived ZrO_2 nanoparticles (R = 30, [HPC] = 2.0 g/l): (a) as-synthesized and (b) calcined at 800 °C for 2 h.

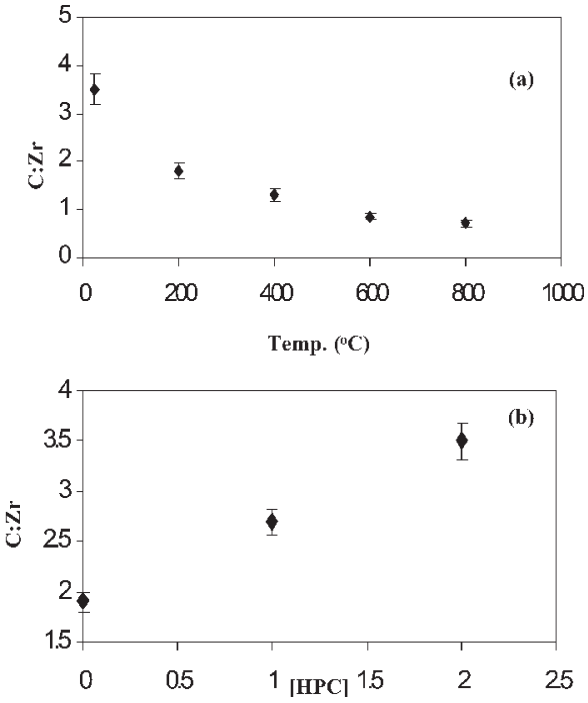

Fig. 4. Variation in C:Zr relative surface atomic ratio, as a function of (a) calcination temperature (R=30,[HPC]=2.0 g/l) and (b) [HPC] (R=30), for the sol-gel derived ZrO_2 nanoparticles.

The variation in the C:Zr relative surface atomic ratio, as obtained from the XPS broad scan analysis, as a function of the calcination temperature and [HPC] is presented in Figs. 4(a) and 4(b) respectively. It is observed that the C:Zr relative surface atomic ratio decreases continuously with increasing calcination temperature, Fig. 4(a). The rate of decrease in the C:Zr relative surface atomic ratio is high within the initial calcination temperature range of 25-400 °C. The rate of decrease, however, decreases significantly above the calcination temperature of 400 °C. On the other hand, the C:Zr relative surface atomic ratio increases linearly with increasing [HPC] within the range of 0.0-2.0 g/l, Fig. 4(b).

Typical SEM micrograph of sub-micron sized ZrO_2 powder synthesized under processing conditions of R=5,[HPC]=1.0 g/l and corresponding broad scan XRD pattern obtained after calcination at 400 °C for 2 h are presented in Figs. 5(a) and 5(b) respectively. Sub-micron sized (~500-600 nm) non-agglomerated spherical ZrO_2 particles are obtained under these processing conditions. The particles are observed to crystallize into tetragonal phase after high temperature calcination. (Note: all nano-sized ZrO_2 powders synthesized in the present investigation were x-ray amorphous and crystallized only at 400 °C). Typical TEM image of nano-sized ZrO_2 powder synthesized under the processing conditions of R=30,[HPC]=0.0 g/l and corresponding broad scan XRD pattern obtained after calcination at 400 °C for 2 h are presented in Figs. 6(a) and 6(b) respectively. The average ZrO_2 nanoparticle size is noted to be ~80-100 nm. These particles also tend to have spherical surface morphology, which is masked by the agglomeration tendency of these particles, Fig. 6(a). These nano-sized ZrO_2 particles crystallize into both tetragonal and monoclinic phases after calcination at 400 °C, Fig. 6(b). Typical TEM image of nano-sized ZrO_2 powder synthesized under the processing conditions of R=30, [HPC]=2.0 g/l and corresponding broad scan XRD pattern obtained after calcination at 400 °C for 2 h are presented in Figs. 7(a)and 7(b) respectively. The average ZrO_2 nanoparticle size is noted to be ~20-25 nm. These particles appear to form 'weak-agglomerates' under these processing conditions, Fig. 7(a) and crystallize into tetragonal crystal structure after calcination at 400 °C, Fig. 7(b). The comparison of Figs. 5-

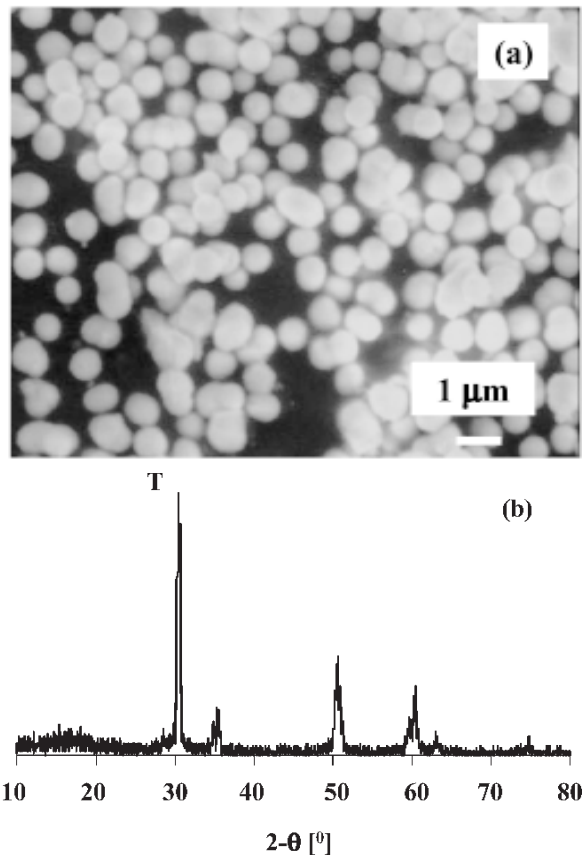

Fig. 5. (a) Typical SEM micrograph showing the sub-micron sized (~500-600 nm), non-agglomerated ZrO_2 particles (*R*=5,[HPC]=1.0 g/l). (b) XRD broad-scan analysis of the particles in (a) after calcination at 400 °C for 2h.

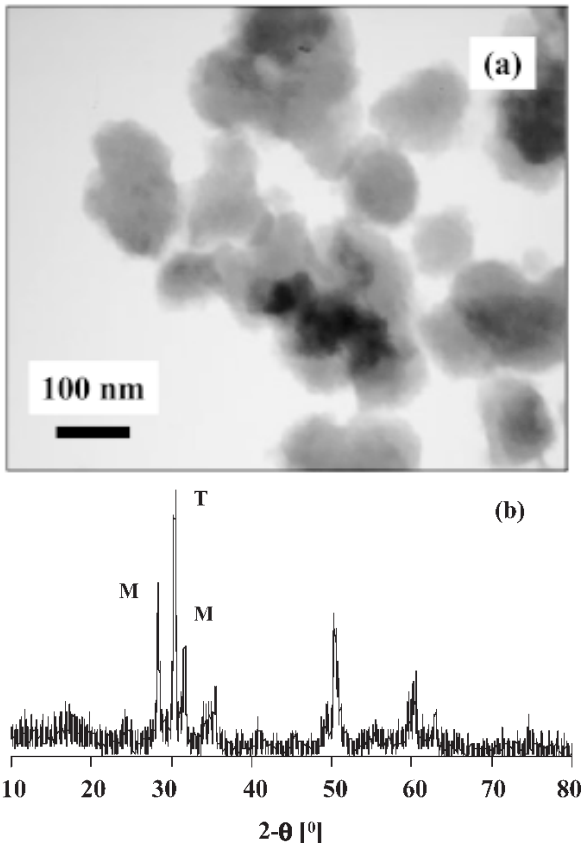

Fig. 6. (a) Typical TEM images showing the nano-sized (~80-100 nm), ZrO_2 particles (*R*=30,[HPC]=0.0 g/l). (b) XRD broad-scan analysis of the ZrO_2 nanoparticles in (a) after calcination at 400 °C for 2h.

7 shows that as-synthesized amorphous ZrO_2 nanoparticles having average particle size of ~500-600 nm, 80-100 nm and 20-25 nm crystallize into only tetragonal, both tetragonal and monoclinic, and only tetragonal phase respectively, after calcination at 400 °C.

HRTEM image obtained from the edge of one of the spherical non-agglomerated ZrO_2 particle, Fig. 5(a), after calcination at 400 °C for 2 h, is shown in Fig. 8(a). The image reveals multiple lattice fringes at the edges of the particles with spacings ranging from ~0.25 to 0.64 nm and non-uniform surface relief with no significant porosity. In addition, small 4-8 nm-sized round-shaped crystalline particles were found at the surfaces of large particles as well. Nanocrystallites of varying shapes and sizes, ranging from 0-100 nm, on the surfaces and in the interior of the particles were observed by dark field TEM. SAED images obtained form the edge and the center of one of the spherical, non-agglomerated ZrO_2 particle, Fig. 5(a), after calcination are shown in Figs. 8(b) and 8(c) respectively. More number of diffraction spots are observed in the SAED pattern obtained from the center of the ZrO_2 particle, Fig. 8(c), than that obtained from the edge of the particle, Fig. 8(b). We, in fact, observed a gradual increase in the number of diffraction spots when traversed from the edge towards the center of the particle. This indicates that a large number of nanocrystallites are located at the center of the particle than that at the particle edge. HRTEM image and corresponding SAED and XRD patterns strongly suggest that the spherical, non-agglomerated ZrO_2 particles are made up of large number of small-sized tetragonal nanocrystallites.

The quantitative phase analysis (i.e. the variation in V_T), at the crystallization temperature of 400 °C, for the sol-gel derived nanocrystalline ZrO_2 powder as a function of '*R*' for various values of [HPC] and MW_{HPC} are presented in Figs. 9(a) and 9(b) respectively. From Fig. 9(a), we observe that, for the [HPC]=0.0 g/l and 1.0 g/l, V_T decreases from

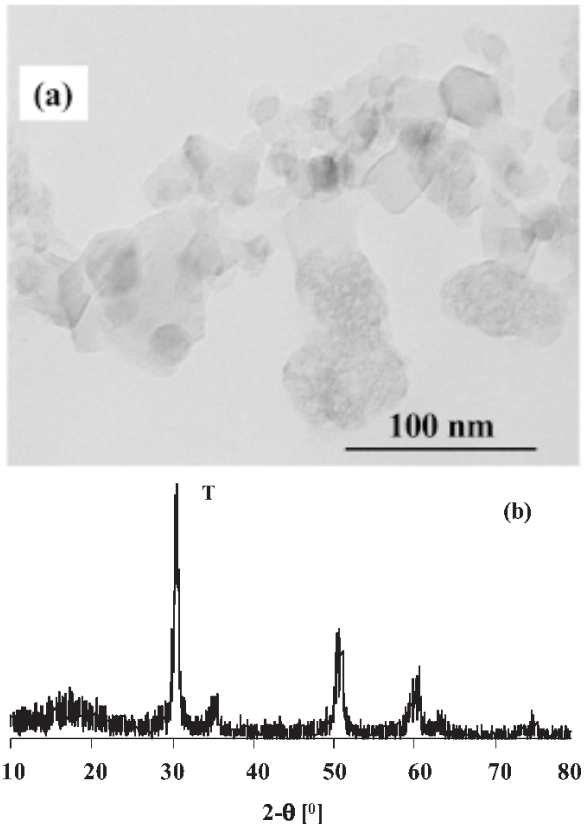

Fig. 7. (a) Typical TEM images of nano-sized (~20-25 nm) ZrO_2 particles (*R*=30,[HPC]=2.0 g/l). (b) XRD broad-scan analysis of the ZrO_2 nanoparticles in (a) after calcination at 400 °C for 2h.

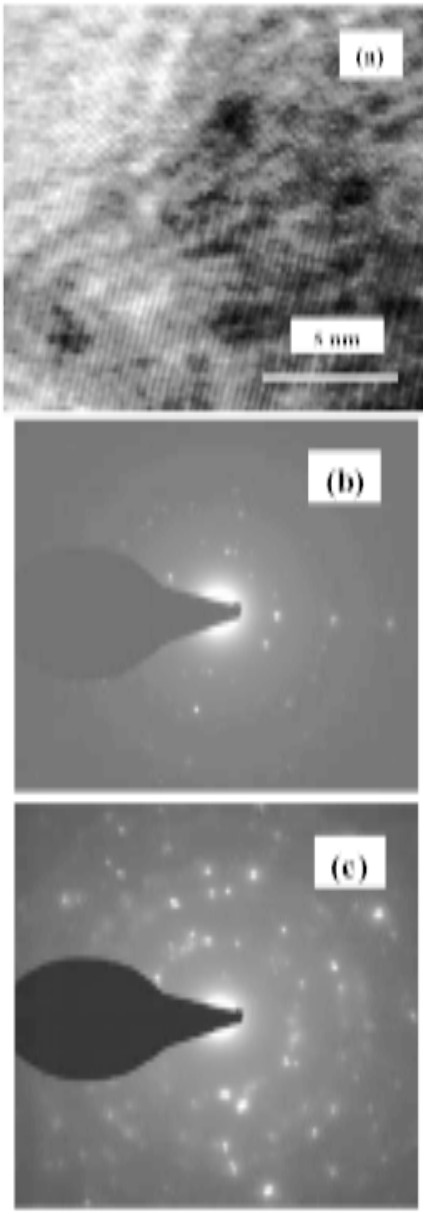

Fig. 8. a) HRTEM image obtained form the edge of one of the sub-micron sized, non-agglomerated, spherical ZrO_2 particle (see Fig. 5(a)) after calcination at 400 °C for 2 h. (b,c) Corresponding SAED patterns obtained from the edge and center of the particle respectively [6,9].

100 to 20-45 % as '*R*' increases within the range of 5-60. On the other hand, 100 % tetragonal phase is observed for all *R*-values, within the range of 5-60, for high [HPC] of 2.0 g/l. Thus, irrespective of '*R*', high [HPC] of 2.0 g/l appears to be a necessary condition for obtaining 100 % tetragonal phase at the crystallization temperature. Moreover, 100 % tetragonal phase can also be obtained in the sol-gel derived nanocrystalline ZrO_2 powder under the processing condition of *R*=5, irrespective of the [HPC]. The effect of MW_{HPC} on the V_T at the crystallization temperature is shown in Fig. 9(b). It is observed that for the nanocrystalline ZrO_2 powder, synthesized in the presence of HPC polymer, ([HPC]=1.0 g/l), V_T decreases from 100% to 40% as '*R*' increases within the range of 5-60. However, the nanocrystalline ZrO_2 powder synthesized in the presence of HPC polymer having molecular weight greater than 80000 g/mol, exhibit 100 % tetragonal phase at the crystallization temperature. This shows that the MW_{HPC} significantly affects the relative volume fractions of nucleating phases at the crystallization temperature and 100 % tetragonal phase can be obtained in the sol-gel derived nanocrystalline ZrO_2 powder when synthesized in the presence of higher molecular weight (>80000 g/mol) HPC polymer, at [HPC]=1.0 g/l.

5. DISCUSSION

5.1. Synthesis of ZrO_2 nanoparticles and role of HPC polymer

The sol-gel synthesis of nano-sized ZrO_2 powder involved the hydrolysis of zirconium (IV) n-propoxide

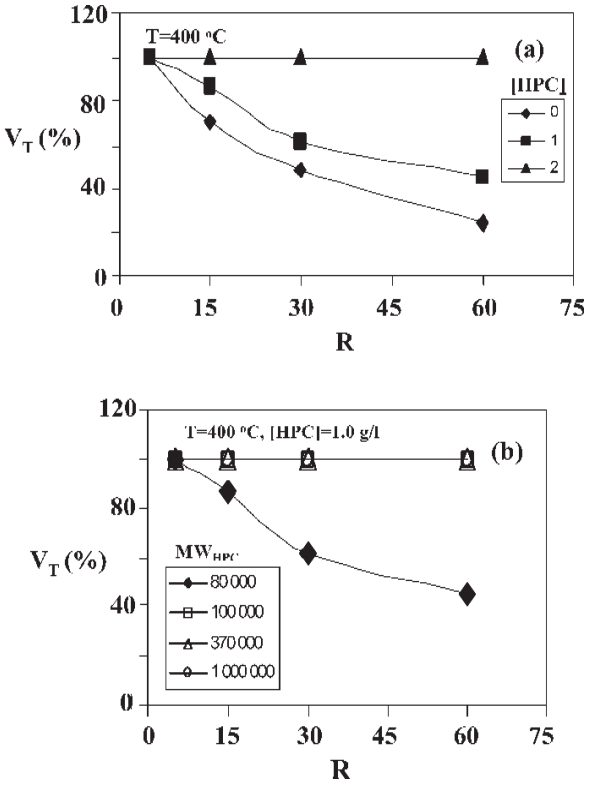

Fig. 9. Variation in the relative volume fraction of metastable tetragonal phase (V_T) as a function of '*R*', for different values of: (a) [HPC] and (b) MW_{HPC}.

in an alcohol solution in the presence of HPC polymer as a steric stabilizer. The hydrolysis and the condensation reactions, which take place as a result of mixing the two parts of alcohol solutions can be described as [5]:

Hydrolysis:

$$Zr(OC_3H_7)_4 + 4H_2O \rightarrow Zr(OH)_4 + 4C_3H_7OH. \quad (3)$$

Condensation:

$$Zr(OH)_4 \rightarrow ZrO_2 + 2H_2O. \quad (4)$$

Net reaction:

$$Zr(OC_3H_7)_4 + 2H_2O \rightarrow ZrO_2 + 4C_3H_7OH. \quad (5)$$

As a result of hydrolysis and condensation reactions, ZrO_2 particles are nucleated in the solution, where the rate of nucleation of particles depends primarily on '*R*' [5]. High water concentrations associated with large *R*-values, result in an increased nucleation rate. As a result, most of the zirconium (IV) n-propoxide hydrolyzes quickly, forming a large number of nuclei. Accordingly, ZrO_2 nanoparticles synthesized in the present investigation, exhibit decrease in the average nanoparticle size for larger *R*-value. The addition of the HPC polymer significantly reduces the agglomeration tendency in the as-synthesized ZrO_2 nanoparticles simultaneously reducing the nanoparticle size. The HPC polymer contains OH^- and ether groups in its structure, which can effectively form hydrogen bonds [15]. ZrO_2 particles, due to their formation via hydrolysis and condensation reactions, exhibit residual OH^- groups on their surface as a result of incomplete condensation reactions at the particle surface. These OH^- groups can take part in the hydrogen bonding with the OH^- groups from the HPC polymer. This type of hydrogen bonding can result in the adsorption of the HPC polymer on the ZrO_2 particle surface, creating a steric hindrance for the particle flocculation within the sol; thus, reducing the particle size in the as-synthesized condition. The formation of sub-micron sized, non-agglomerated ZrO_2 particles is also attributed to the adsorption of the HPC polymer over the surface of ZrO_2 particles.

5.2. Mechanisms of metastable tetragonal phase stabilization in nano-sized ZrO_2

During the crystallization process, the phase evolution from the amorphous ZrO_2 follows the sequence of [5]: Amorphous → Tetragonal → Tetragonal + Monoclinic → Monoclinic. According to this phase evolution sequence, it is the tetragonal phase, which crystallizes first from the amorphous phase. According to Shukla et al. [6], the metastable tetragonal phase can be stabilized within the sub-micron sized ZrO_2 particles provided they consist of 'hard-aggregates' of small nanocrystallites, which can effectively prevent the tetragonal-to-monoclinic phase transformation, which is always accompanied by volume expansion; thus preventing the phase transformation process. The stabilization of metastable tetragonal phase within the sub-micron sized (~200 nm and 500-600 nm), agglomerated/non-agglomerated ZrO_2 particles is due to the 'aggregation-mechanism', Fig. 10 (a). On the other hand, the ZrO_2 nanoparticles having the average nanoparticle size of ~80-100 nm exhibit tetragonal-to-monoclinic phase transformation during the phase evolution process. The strain energy associated the interface boundary stabilizes the metastable tetragonal phase in this case, Fig. 10(b), which is according to the 'strain-energy' theory proposed by Mitsuhashi et al. [16]. According to Garvie [17], however, the ZrO_2 nanoparticle size of less than 30 nm is thermodynamically favorable for the stabilization of metastable

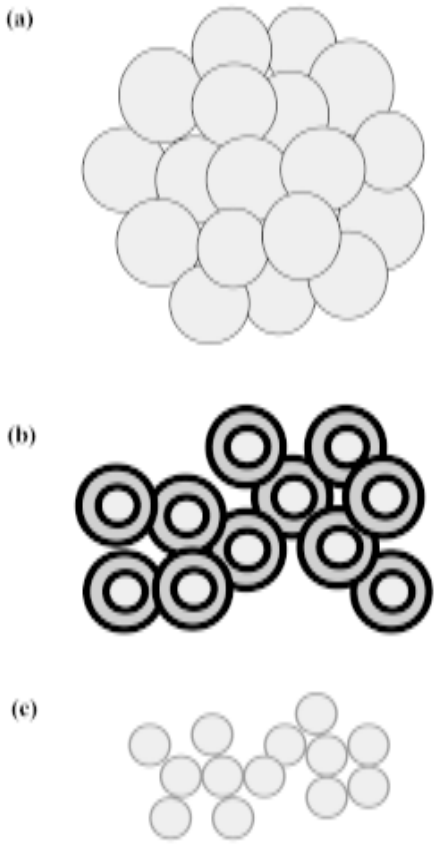

Fig. 10. Schematic diagram showing three different mechanisms responsible for the stabilization of metastable tetragonal phase in sub-micron sized (a) and nanocrystalline (b,c) ZrO_2. 'Aggregation' (a), 'strain-energy' (b), and 'particle-size' mechanisms (c) are observed for the average ZrO_2 particle size of >200 nm, ~80-100 nm, and <30 nm respectively. Shaded area – tetragonal phase and dark area – monoclinic phase.

tetragonal phase. Hence, according to this theory, in this investigation, the metastable tetragonal phase is stabilized for ZrO_2 nanoparticles having the average nanoparticle size of ~20-25 nm, Fig. 10(c). Thus, it appears that the average ZrO_2 nanoparticle size and their aggregation tendency both critically affect the metastable tetragonal phase stabilization in ZrO_2 nanoparticles.

5.3. Dependence of phase evolution behavior on *R*, [HPC], and MW_{HPC}

The variation in V_T as a function of *R*, [HPC], and MW_{HPC}, as observed in the present investigation, can be explained on the basis of above-mentioned three different mechanisms responsible for the metastable tetragonal phase stabilization in nano-sized ZrO_2. The two of the three mechanisms, namely the 'aggregation-mechanism' and 'particle-size effect', stabilizes only the tetragonal phase. On the other hand, the 'strain-energy' mechanism involves the formation of monoclinic phase as well.

When ZrO_2 particles are synthesized under low *R*-value (=5), the sub-micron sized particles are invariably formed and the 'aggregation-mechanism' stabilizes the only tetragonal phase within these particles at the crystallization temperature. With increase in *R*-value ([HPC]=0.0 g/l), the nucleation rate of ZrO_2 nanoparticles increases, and as a result, the volume fraction of sub-micron sized particles decreases with increasing '*R*'. Moreover, it appears that the ZrO_2 nanoparticles having average nanoparticle size of ~80-100 nm is ineffective for the operation of 'aggregation-mechanism'. As a result, the tetragonal-to-monoclinic transformation occurs in these particles. The increase in the volume fraction of nanoparticles (~80-100 nm) at the expense of that of sub-micron sized particles (that is, decrease in the average particle size) with increasing *R*-value, is possibly responsible for increase in the volume fraction of monoclinic phase with increasing '*R*'. Thus, the 'strain-energy' mechanism primarily operates at higher *R*-value (=30) while the 'aggregation-mechanism' dominates at lower *R*-value (=5). Beside this, the operating mechanism responsible for the metastable tetragonal phase stabilization changes again due to addition of the HPC polymer. As mentioned earlier, the HPC polymer gets adsorbed on the particle surface during processing and provides steric hindrance for particle-particle aggregation. As a result, the average ZrO_2 nanoparticle size is restricted below ~30 nm as observed for the addition of [HPC]=2.0 g/l. Hence, the 'particle-size' effect becomes a dominant mechanism when the HPC polymer is added during the processing of ZrO_2 nanoparticles. The stabilization of only tetragonal phase, as observed for [HPC]=2.0 g/l, is attributed to this phenomenon. Thus, the variation in V_T as a function of *R* and [HPC] is attributed to the variation in average particle size with respect to the variation in *R* and [HPC], which in turn changes the mechanism of metastable tetragonal phase stabilization in nano-sized ZrO_2 particles. It also appears that an increased level of branching associated with an increasing MW_{HPC} is probably responsible for providing enhanced steric hindrance against particle coalescence; thus, stabilizing the 100 % metastable tetragonal phase for larger values of MW_{HPC} (>80000 g/mol).

6. CONCLUSIONS

(1) Nanocrystalline as well as sub-micron sized ZrO_2 powder has been successfully synthesized using sol-gel technique, utilizing the HPC polymer as a steric stabilizer.

(2) There are three different mechanisms responsible for the metastable tetragonal phase stabilization in nanocrystalline undoped ZrO_2.

(3) During the crystallization process from the amorphous phase, within the nano-sized ZrO_2 powder, the metastable tetragonal phase stabilization takes place by 'particle-size', 'strain-energy', and 'aggregation' mechanisms only if the as-synthesized average ZrO_2 nanoparticle size is <30 nm, ~80-100 nm, >200 nm, respectively.

(4) The variation in the relative volume fraction of metastable tetragonal phase as a function of *R* and [HPC] is attributed to the variation in the average particle size with respect to the variation in *R* and [HPC], which changes the mechanism of metastable tetragonal phase stabilization.

ACKNOWLEDGEMENTS

Authors thanks Energy Strategy Inc. (U.S.A.) and Coal Resources Inc. (U.S.A.), and National Science Foundation EEC 0136710, 0085639, for financial support. Authors thank Prof. Vladimir Oleshko (University of Virginia) for conducting HRTEM analysis.

REFERENCES

[1] D.L. Porter, A.G. Evans and A.H. Heuer // *Acta Metall.* **27** (1979) 1649.

[2] M. Haruta, T. Kobayashi, H. Sano and N. Yanada // *Chem. Lett.* **829** (1987) 405.

[3] R.S. Pavlik Jr., L.C. Klein and R.A. McCauley // *J. Am. Ceram. Soc.* **78** (1995) 221.

[4] E. Haefele, K. Kaltenmaier and U. Schoenauer // *Sensors and Actuators B: Chemical* **B4** (1991) 525.

[5] S. Shukla, S. Seal and R. Vanfleet // *J. Sol-Gel Sci. Technol.* **27** (2003), in press.

[6] S. Shukla, S. Seal, R. Vij, S. Bandyopadhyay and Z. Rahman // *Nano Letters* **2** (2002) 989.

[7] S. Shukla, S. Seal, R. Vij and S. Bandyopadhyay // *J. Nanoparticle Research* (2002), in press.

[8] S. Shukla and S. Seal, In: *Proceedings of TMS Annual Meeting, Surface Engineering in Materials Science – II* ed. by S. Seal, N.B. Dahotre, J. Moore, A. Agarwal and S. Suryanarayana (San Diego, CA, 2003), in press.

[9] V.P. Olleshko, J.M. Howe, S. Shukla and S. Seal // *J.Am. Ceram Soc.* (communicated).

[10] G. Beamson and D. Briggs, *High Resolution XPS of Organic Polymers* (Wiley & Sons, New York, 1992).

[11] T.L. Barr and S. Seal // *J. Vac. Sci. Tech. A* **13** (1995) 1239.

[12] P.M.A. Sherwood, In: *Practical Surface Analysis Second Edition Vol. 1 – Auger and Photoelectron Spectroscopy, Appendix 3*, ed. by D. Briggs and M.P. Seah, (Wiley, New York, 1996), p. 555.

[13] M.I. Osendi, J.S. Moya, C.J. Serna and J. Soria // *J. Am. Ceram. Soc.* **68** (1985) 135.

[14] B.D. Cullity, *Elements of X-Ray Diffraction* (Addison-Wesley, MA, 1978), p.102.

[15] S. Shukla, S. Seal and S. Mishra // *J. Sol-Gel Sci. Technol.* **23** (2002) 151.

[16] T. Mitsuhashi, M. Ichiara and V. Tatsuke // *J. Am. Ceram. Soc.* **57** (1974) 97.

[17] R.C. Garvie // *J. Phys. Chem.* **69** (1965) 1238.